The Cryosphere Discuss., doi:10.5194/tc-2016-229, 2016
Manuscript under review for journal The Cryosphere
Published: 1 November 2016

The Cryosphere Discussions
Open Access
EGU

Resolution capacity of geophysical monitoring regarding permafrost degradation induced by hydrological processes

Benjamin Mewes[1], Christin Hilbich[2], Reynald Delaloye[2], Christian Hauck[2]

[1]Institute of Hydrology, Water Resources Management and Environmental Engineering, Ruhr-University Bochum, Bochum, 44801, Germany
[2]Department of Geosciences, University of Fribourg, Fribourg, 1700, Switzerland

Correspondence to: Benjamin Mewes (Benjamin.Mewes@rub.de)

Abstract. Geophysical methods are often used to characterise and monitor the subsurface composition of permafrost. The resolution capacity of standard methods, i.e. Electrical Resistivity Tomography and Refraction Seismic Tomography, depends hereby not only on static parameters such as measurement geometry, but also on the temporal variability in the contrast of the geophysical variables (electrical resistivity and P-wave velocity). Our study analyses the resolution capacity of Electrical Resistivity Tomography and Refraction Seismic Tomography for typical processes in the context of permafrost degradation using synthetic and field data sets of mountain permafrost terrain. In addition, we tested especially the resolution capacity of a petrophysically-based quantitative combination of both methods, the so-called 4-phase model, and by this analysed the expected changes in water and ice content upon permafrost thaw. The results from the synthetic data experiments suggest a higher sensitivity regarding increasing water content compared to decreased ice content, and potentially larger uncertainty for the individual geophysical methods than for the combined evaluation with the 4-phase model. In the latter, ground ice loss can be detected quite reliably, whereas artefacts occur in the case of increased horizontal or vertical water flow. Analysis of field data from a well-investigated rock glacier in the Swiss Alps successfully visualised the seasonal ice loss in summer, and the complex spatially variable ice-, water- and air content changes in an interannual comparison.

1 Introduction

Geophysical methods are frequently applied for the investigation of mountain permafrost (Hauck and Kneisel, 2008). In particular Electrical Resistivity Tomography (ERT) and Refraction Seismic Tomography (RST) are well suited to differentiate between frozen and unfrozen conditions (for reviews see Scott et al., 1990; Kneisel et al., 2008; Hauck, 2013). In monitoring applications, ERT and RST allow to resolve phase changes between liquid water and ice as well as saturated and unsaturated conditions over a wide range of temporal and spatial resolutions (e.g. Hilbich et al., 2008; Hilbich et al., 2011, Maurer and Hauck, 2007; Krautblatter et al., 2010; Hilbich, 2010; Kneisel et al., 2014; Supper et al., 2014; Dräbing, 2016).

The Cryosphere Discuss., doi:10.5194/tc-2016-229, 2016
Manuscript under review for journal The Cryosphere
Published: 1 November 2016

Among the various types of landforms in which mountain permafrost is occurring, rock glaciers occupy a specific place, partly due to their role as permafrost indicator that can be easily detected in the landscape and due to their kinematic behaviour with movement rates typically ranging from a few centimetres up to several metres per year. The increase in creep velocities observed for many rock glaciers in the European Alps for the last 20-30 years, and in particular for the last decade (e.g. Kellerer-Pirklbauer and Kaufmann, 2012; Delaloye et al., 2008; 2010; PERMOS, 2016), makes the investigation of the role of liquid water for the dynamics of rock glaciers more and more important (e.g., Haeberli et al., 2006; Jansen and Hergarten, 2006; Krainer and Mostler, 2002). It has been assumed that the thermal and hydro-mechanical effects of water infiltration may significantly control the seasonal and short-time pattern of creep velocities, e.g. by the reduction of shear resistance by infiltrated melt water (e.g. Krainer and He, 2006; Perruchoud and Delaloye, 2007; Ikeda et al., 2008). Whereas water infiltration at the surface of rock glaciers could be estimated by means of indirect interpretation of ground thermal regimes (e.g. Humlum, 1997; Sawada et al., 2003; Staub and Delaloye, 2016), in-situ measurements are rare, in particular because a standard sensor deployment is often difficult due to the coarse-grained surface layer (Buchli et al., 2013). To our knowledge, direct measurements of water infiltration into the permafrost body are inexistent so far. Indirect methods such as geophysical techniques (e.g. ERT and RST, but also Nuclear Magnetic Resonance (NMR) and self-potential (SP), see Hauck, 2013) could in principle help to estimate the liquid water content within the permafrost body and to identify preferential flow paths (Scapozza et al., 2008; Scherler et al., 2010; Lehmann-Horn et al., 2011; Voytek et al., 2016). They can also efficiently be used to monitor permafrost changes over time (e.g. Hilbich et al., 2011). However, the resolution capacity of geophysical data for localised anomalies such as preferential flow paths of melt water through permafrost and talik formation depends on various factors such as depth of the anomaly, resistivity/velocity contrasts and measurement geometry. A reliable interpretation of small scale geophysical anomalies (or their temporal changes) remains therefore difficult (Hilbich et al., 2009). Current challenges for the application of geophysical methods to rock glaciers include a) the resolution potential for small-scale anomalies/processes (ideally down to the depth of the shear horizon at 15-20 m or more), and b) the delineation of the complex internal structure and the quantification of the overall ice/water content in a rock glacier (Maurer and Hauck, 2007; Monnier et al., 2011; Monnier and Kinnard, 2013; Hausmann et al., 2007; Merz et al., 2015).

The aim of this study is to analyse the qualitative and quantitative resolution potential of repeated geophysical measurements (ERT and RST) for the monitoring of hydrological and glaciological processes with a focus on snow melt infiltration and ice melt. The resolution potential of ERT and RST for the monitoring of hydrological processes in the context of permafrost degradation within rock glaciers is analysed using synthetic models with simplified geometries simulating idealized water flow paths and ice loss scenarios. In a next step, we combine the results from both methods to run a petrophysical model, which estimates the quantitative distribution of ice and water contents within the rock glacier (Hauck et al., 2011). With this so-called 4-phase model (4PM) and various (synthetic) scenarios of changes in ice and water content we investigate the performance of the 4PM regarding its spatial resolution capacity, the latter being partly a function of the individual resolution capacities of ERT and RST.

The Cryosphere Discuss., doi:10.5194/tc-2016-229, 2016
Manuscript under review for journal The Cryosphere
Published: 1 November 2016

Finally, the results will be analysed in comparison with real field data from the Becs-de-Bosson rock glacier, ~~a well-investigated rock glacier in the Swiss Alps (e.g. Tenthorey, 1993)~~. Data from repeated ERT and RST surveys are used to model the volumetric fractions of ice, water and air with the 4PM. Geophysical input data and 4PM results are analysed with respect to their qualitative resolution potential regarding processes related to snow melt infiltration and ice degradation during a 2-year period from 2012 to 2013.

2 Field site and available data

The Becs-De-Bosson rock glacier (cf. Figure 1) is the biggest active rock glacier in the Val de Réchy, Western Swiss Alps. It covers an area of 246.000 m² in NW exposition over an altitudinal range between 2'620 – 2'850 m asl. The rock glacier is mainly consisting of calc-schist debris, whereas the landform is extending over a basement of quartzite and gneiss locally superimposed by evaporitic rocks (dolomite, gypsum) (Tenthorey, 1993). The measured mean annual air temperature on the rock glacier is -1 °C (1997-2014), which is approximately 1 – 1.5 °C warmer than in the decades prior to the 1980s (according to available long-term time series in the Swiss Alps, www.meteoswiss.ch). Most of the precipitation falls as snow from October to May, constituting a snowpack that frequently overpasses 2 meters before the beginning of the melt season in early May. In early July, the snow has usually completely disappeared on most of the rock glacier, while some snow patches may persist in the rooting zone until end of summer.

Large parts of the rock glacier rooting zone contain no permafrost due to the presence of a glacier during the Little Ice Age (Tenthorey, 1993; Delaloye, 2004). The rock glacier tongue is still frozen and affected by permafrost creep. The active layer is estimated to be about 4 m thick along the frozen section and consists of small debris mixed with big boulders (Tenthorey, 1993; Delaloye, 2004). Creep rates are very heterogeneous but gradually decreasing downwards from about 2.4 m/a (in 2012-2013) in the central part to 0.3 m/a near the rock glacier tongue. After the average creep velocity had already doubled between the 1980s and the early 2000s (Kääb, 2005; Perruchoud and Delaloye, 2007), GNSS surveys revealed a continuous velocity increase in recent years for selected points along the ERT/RST profile (Figure 1). This increase showed values from 0.43 m/a in 2006 (range: 0.19 – 0.68 m/a) to about 1.00 m/a in 2010-2012 (range: 0.30 – 2.00 m/a), and finally 1.43 m/a in 2015 (range: 0.40 – 2.89 m/a). Seasonal creep velocity analysis revealed an acceleration during the time of snow melt (Perruchoud and Delaloye, 2007), and a drop in creep velocity in July followed by an acceleration phase in late summer.

Repeated ERT and RST surveys are conducted along a longitudinal profile reaching from the rooting zone (no permafrost) across the rock glacier tongue (cf. Figure 1) with the aim to investigate the change of its spatial ground ice distribution and the influence that ice and liquid water content may have on its kinematic behaviour. For this study, coincident ERT and RST data from 21 July 2012, 25 July 2013 and 27 September 2013 were used. ERT data were collected with a GeoTom instrument (Geolog, Augsburg) along 71 permanently installed electrodes with 4.5 m spacing using the Wenner and Wenner Schlumberger configuration. Galvanic coupling was good with contact resistances < 50 Ωm for every electrode. However, data misfit (absolute error in the inversion, see below) was still between 6.9 – 14 % after four iterations illustrating the

The Cryosphere Discuss., doi:10.5194/tc-2016-229, 2016
Manuscript under review for journal The Cryosphere
Published: 1 November 2016

difficult measurement conditions on a rock glacier. They are nevertheless comparable to similar surveys on rock glaciers presented in previous studies (e.g, Marescot et al., 2003; Hilbich et al., 2009, Maurer and Hauck, 2007). The RST data were measured with a Geode24 instrument (Geometrics) in roll-along mode using 43 receiver locations with 4.5 m spacing and 28 shot locations. Generally, about 15-20 individual shots were stacked at each shot point location to ensure good data quality for first-arrival picking. Shot points and geophone locations were marked and measured by dGPS to reduce the geometric error by the repeated surveys. The overlapping part of the slightly shifted ERT and RST profiles used for the 4PM calculation yields an overall length of 160 m.

According to ground surface temperature (GST) measurements since 2000 snow melt was completed about 8-15 days later in 2013 than in 2012 (16 June 2013 vs. 08 June 2012 at a snow-poor location close to the lower end of the profile; 24 July 2013 vs. 08 July 2012 at a snow-rich location close to the upper part of the profile). Measured precipitation between June and October was similar for the two years (300 mm in 2012 and 350 mm in 2013.

Several streamlets with permanent or episodic discharge are emerging alongside the rock glacier front. According to continuous discharge time series recorded from 1992 to 2001 the total discharge is maximal during the snow melt season (May-July) and drastically decreasing thereafter (Gardaz, 1999). Rainfall may produce some short-stage peak discharge events during the snow free period. Tracer experiments by Tenthorey (1993, 1994) and Mari et al. (2012) from the rooting zones of the Becs-de-Bosson and Tsavolires (at 0.5 km distance) rock glaciers showed that i) the residence time of water in the rock glacier hydrological system is relatively long and highly variable ranging mostly from several days to several months to pass the linear distance of 0.6 km from the rooting zone to the tongue, ii) the main flow path is developing beneath the permafrost body or in taliks (presumably close to the contact of the frozen sediments to the bedrock), and iii) there is a strong mixing (in- and outflow) with other porous or fissure/karstic groundwater systems. Even if the internal structure controlling the flow paths of infiltrated water in the rock glacier is still unknown, both discharge times series and results of tracer experiments support the hypothesis assuming that aquifer conditions exist at the base of the rock glacier and that rising groundwater table may influence its creep rate during the snow melt season.

3 Methods

3.1 Geophysical monitoring and forward-inverse modelling cycles

Geophysical techniques such as refraction seismic tomography and electrical resistivity tomography are suitable field methods to gain a better understanding of (invisible) subsurface processes ~~from the surface of the landform~~ (e.g. infiltration of meltwater or degradation of ground ice) (Hilbich et al., 2009; Merz et al., 2015). Their non-invasive nature also allows repeated measurements of the same profile (Hilbich, 2010; Hilbich et al., 2011; Kneisel et al., 2014), which can considerably improve the identification of hydrological processes in alpine permafrost systems (Langston et al., 2011; Wright et al., 2009) as well as in non-permafrost catchments (Kobierska et al., 2015) and for 1-D infiltration studies (Scherler et al., 2010). Rock glaciers, however, belong to the most challenging landforms for geophysical monitoring. Firstly, their rough surface

The Cryosphere Discuss., doi:10.5194/tc-2016-229, 2016
Manuscript under review for journal The Cryosphere
Published: 1 November 2016

characteristics consisting of very coarse-grained material and boulders, and their small-scale topography and high ice contents make good-quality measurements and data inversions difficult (Hilbich et al., 2009; Hauck and Vonder Mühll, 2003), and secondly, the movement of the landforms disturbs permanent installations and significantly alters the measurement geometry with time (Wilkinson et al., 2010; Loke et al., 2013).

Hilbich et al. (2009) demonstrated the general applicability of repeated ERT surveys to monitor permafrost evolution on rock glaciers and also highlighted the use of synthetic modelling to aid the sometimes ambiguous interpretation of the results. A systematic use of synthetic modelling in so-called forward-inverse-cycles was presented by Fortier et al. (2008) and Kneisel et al. (2008) to ameliorate the process of data acquisition, inversion and interpretation for geophysical investigations in alpine or arctic settings. The forward-inverse-cycle describes the process of acquiring, inverting and interpreting geophysical data (Fortier et al., 2008, see also Figure 2). It gives detailed feedback for every step in the sequence of a geophysical investigation and allows the amelioration of measurement set up and data interpretation.

Forward-inverse cycles consist not only of the standard geophysical inversion step, which inverts the measured data by a mathematical relationship to yield the distribution of specific properties of the subsurface (in our case specific electrical resistivity (for ERT) and seismic P-wave velocity (for RST)), but also of an additional forward calculation which predicts a set of geophysical measurement data based on a synthetic subsurface model with specific model parameters. Forward modelling of a synthetic model thus allows us to generate synthetic measurement data sets, which can then be inverted to investigate the response of the complete measurement/inversion procedure to a given subsurface structure and measurement geometry. By this, the potential resolution of structures and processes of interest as well as the unwanted occurrence of inversion artefacts can be analysed (e.g. Hilbich et al., 2009).

In this study we use forward-inverse cycles to compare the inversion results of synthetic data sets to the inversion results of real field data as well as to analyse the potential resolution of three geophysical approaches regarding processes which are relevant for permafrost degradation: (1) ERT alone, (2) RST alone and (3) ERT & RST combined in the 4-phase model. Whereas forward-inverse cycles for permafrost applications have already been introduced in previous studies (Fortier et al., 2008; Kneisel et al., 2008; Hilbich et al., 2009) a forward-inverse based appraisal of a combination of methods (as in the 4PM) has never been attempted before.

3.2 Work flow

Figure 2 illustrates the main steps in the work flow applied in this study. The measured field data (apparent resistivities and travel times) are inverted in step 1 to obtain tomograms with the spatial distribution of specific resistivities and p-wave velocities. These models are the starting point for setting up synthetic reference models in step 2. These reference models were chosen to be ~~a)~~ consistent with the measured data of step 1, as well as ~~b)~~ simplified regarding geometry and small-scale structure to use them as a starting point for various scenarios. A simplified subsurface structure was constructed from the inverted field data, and realistic values for ρ_s and v_p were assigned to all layers ~~(see next section)~~. These values were taken from literature (cf. Table 1) and adapted in order to fit the inverted field data as best as possible.

The Cryosphere Discuss., doi:10.5194/tc-2016-229, 2016
Manuscript under review for journal The Cryosphere
Published: 1 November 2016

Synthetic data sets of ρ_a and seismic travel times were generated from the reference models through forward modelling applying the same measurement geometry as for the field data, and were subsequently inverted using the same inversion parameters as in step 1. Through comparison of the inverted tomograms of synthetic models and field data and repetition of the sub-cycle consisting of forward, inverse and appraisal problem (step 2), the synthetic models can iteratively be adapted until they produce tomograms of ρ_s and v_p, which correspond to those of the field data within acceptable bounds (step 3).

In a next step three modifications of the baseline synthetic model were developed ~~(see next section)~~ to represent typical mountain permafrost processes in the context of degradation. In the second part of the study, the ERT and RST tomograms of these 3 scenarios will then serve as input into the 4PM (step 4) and the individual fractions of ice, water and air will be calculated from ~~a)~~ the geophysical values in the synthetic models, ~~b)~~ the inverted synthetic models and ~~c)~~ from the inverted field data. Finally, the results of the 4PM for all 3 approaches will be compared and analysed regarding their resolution capacity for the different processes represented in the three scenarios (step 5).

3.3 Synthetic models and data inversion

The synthetic models were created based on the interpretation of the real field data from the Bec de Bosson rock glacier. Figure 3a shows the tomograms of ERT (top) and RST (bottom) measurements from 25 July 2013, with black lines representing the individual interpretation of the tomograms. Certain layers are visible in both tomograms, but the two methods also deliver complementary information. Layer 1 is clearly detected by both methods and is interpreted as the active layer consisting of coarse blocks. However, this layer is considerably thinner in the ERT (about 3-6 m) than in the RST tomogram (5-10 m). In the upslope part of the profile the active layer is characterized by lower resistivities and partly also lower velocities, which is interpreted as finer grained material with higher moisture content (layer 2). Layer 3 denotes an ice-rich layer with roughly 10 m thickness, which is very prominent in the ERT data (very high resistivities of >100 kΩm), but also visible in the RST data (~3500 m/s). Towards the upslope part both resistivity and velocity gradually decrease and indicate decreasing ice content. Zones 4 and 5 are therefore interpreted as ice-poor and ice-free zones with similar thickness, zone 4 can however rarely be identified in the RST data. Whereas both methods give clear indications, that the bedrock is present at approximately 15 m depth, only the seismic method is able to delineate the details of the bedrock topography.

The structure and geophysical properties of these layers are then translated into the baseline synthetic model (SYN1) with the aim to reproduce the observed subsurface composition with a simplified structure. Figure 3b (top panel) shows the resulting model: an active layer, an intermediate layer with 3 lateral zones of different ice contents (ice-rich, ice-poor, no ice), and the bedrock at the bottom of the profile.

Based on this baseline model three different scenarios are set up:

- SYN2: A saturated 1.5 m thick layer on top of the ice core
- SYN3: three 0.5 m wide vertical preferential flow paths, of which one crosses the ice core. All flow paths end up in a horizontal saturated layer at 10m depth, which flows beneath the ice core
- SYN4: a degradation of the ice core by 2 m thickness from above

The Cryosphere Discuss., doi:10.5194/tc-2016-229, 2016
Manuscript under review for journal The Cryosphere
Published: 1 November 2016

Whereas SYN4 represents the classical permafrost degradation scenario (see e.g. Hilbich et al., 2009) scenarios SYN2 and SYN3 depict two hydrological situations that were hypothesised for rock glaciers within the seasonal cycle of thawing and freezing (e.g. Ikeda et al., 2008; Arenson et al., 2010; Duguay et al., 2015): The development of preferential flow paths during the snow-melt season (SYN3), and resulting saturated layers of melt and rain water on permanently frozen areas like the ice core (SYN2).

The geophysical properties in the synthetic models are further assigned in the forward modelling module of ReflexW (for seismic data, Sandmeier, 2015) and the data generator RES2DMOD (for ERT data, Loke, 2002). As the geoelectric forward modeling software RES2DMOD does not allow topography, no topography will be used in both synthetic models. By forward modelling all synthetic models are translated into virtual measurement data with 5% Gaussian noise added to simulate real (i.e. non-ideal) field data. The resulting synthetic measurement data are inverted using RES2DINV (Loke, 2015) and ReflexW (Sandmeier, 2015) software using a robust L2-Gauss-Newton-Inversion for the geoelectric data (and standard inversion parameters as described in (Hilbich et al., 2009), and the simultaneous iterative reconstruction technique for the seismic data (inversion parameters chosen according to Hilbich (2010).

3.4 4-phase model (4PM))

The 4PM is a petrophysical model that relates specific electrical resistivities and seismic P-wave velocities by two well-known petrophysical mixing rules (Archie, 1942; Timur, 1968) to obtain volumetric fractions of air, water, ice and rock (Hauck et al., 2011). As electrical resistivities are well suited to differentiate between ice and water, and seismic velocities are sensitive to transitions between air and ice or rock, the combination of these methods is in principle suitable for estimating the lateral heterogeneity and quantifying the volumetric contents of ice-rich bodies in a rock glacier. The model has already been successfully applied to alpine permafrost bodies (Hauck et al., 2011; Schneider et al., 2013; Pellet et al., 2016) and uses the following equations to determine the volumetric ice (f_i), water (f_w) and air content (f_a) for a given porosity model Φ (x,z) ($\Phi = 1 - f_r$; f_r being the rock content):

$$f_w = \left(\frac{a\rho_w (1-f_r)^n}{\rho (1-f_r)^m} \right)^{1/n} \quad (1)$$

$$f_i = \frac{v_i v_a}{v_a - v_i} \left[\frac{1}{v} - \frac{f_r}{v_r} - \frac{1-f_r}{v_a} + \left(\frac{a\rho_w (1-f_r)^n}{\rho (1-f_r)^m} \right)^{1/n} \left(\frac{1}{v_a} - \frac{1}{v_w} \right) \right] \quad (2)$$

$$f_a = \frac{v_i v_a}{v_i - v_a} \left[\frac{1}{v} - \frac{f_r}{v_r} + \frac{1}{v_i} (f_r - 1) - \left(\frac{a\rho_w (1-f_r)^n}{\rho (1-f_r)^m} \right)^{1/n} \left(\frac{1}{v_w} - \frac{1}{v_i} \right) \right] \quad (3)$$

The Cryosphere Discuss., doi:10.5194/tc-2016-229, 2016
Manuscript under review for journal The Cryosphere
Published: 1 November 2016

where a (= 1 in many applications), m (cementation exponent) and n (saturation exponent) are empirically determined parameters (Archie, 1942), ρ_w is the resistivity of the pore water, v_r, v_w, v_a, v_i are the theoretical P-wave velocities of the four components, and $\rho\ (x,z)$ and $v\ (x,z)$ are the inverted resistivity and P-wave velocity distributions, respectively. The free parameters in Equations (1) - (3) are the so-called Archie parameters n, m and ρ_w, the seismic velocities of the four materials and especially the porosity distribution Φ (x,z), the latter being estimated as direct measurements rarely exist. Values for the seismic velocities v_w, v_a, v_r and v_i as well as n and m are taken from literature (Schön, 2015; Knödel et al., 2013; Zimmerman and King, 1986) (see Tab. 2). The highly sensitive parameter ρ_w (Hauck et al., 2011) was estimated using experience from various electrical conductivity measurements in alpine permafrost regions (unpublished). 4PM plausibility check is achieved by verifying if physically consistent solutions are available for a specific data pair of ρ_s and v_p and the parameter specified (e.g. sum of f_i, f_a and f_w is $\leq \Phi$, and all volumetric contents are ≤ 0).

The resulting ice-, water- and air content distributions can then be analysed as absolute values or saturation values relative to the available pore space, the latter being less dependent on uncertain porosity models. For the field and synthetic examples of this study, volumetric contents are displayed as changes to the baseline model SYN1 to illustrate the different processes of the scenarios (SYN2, SYN3, SYN4).

In this paper we conducted three different steps to evaluate the performance of the 4PM:

a) we run the 4PM using the *pure synthetic models* (without inversion) as a demonstration of the proof-of-concept of the 4PM,
b) we use the *inverted synthetic models* as input for the 4PM to analyse the general performance of the 4PM,
c) from a) and b) we identify primary *error sources* of the model and attribute them to either the input data or the 4PM itself. By comparing both input data types the resolution capacity of the different geophysical methods as well as the occurrence of inversion artefacts become apparent. The resolution capacity of *temporal changes* in the subsurface conditions is then examined by a time-lapse analysis which compares 4PM results of the 3 scenarios to the baseline model.

4 Results

4.1 Analysis of synthetic geophysical monitoring data

4.1.1 Synthetic models

Figure 4 a,b show the ERT and RST synthetic models for the baseline and the scenario experiments. By subtracting the baseline model SYN1 from all scenarios the resistivity and velocity changes for the various scenarios are determined (Figure 4 c,d). An appearance of a water saturated layer on top of the ice core would therefore result in a decrease in resistivity (red horizontal bar in SYN2), but an increase in P-wave velocity (blue bar in SYN2). Ice loss (SYN4) can be detected by a

The Cryosphere Discuss., doi:10.5194/tc-2016-229, 2016
Manuscript under review for journal The Cryosphere
Published: 1 November 2016

contemporaneous decrease in resistivity and velocity, and the preferential flow pattern would be visible by resistivity decrease and velocity increase in the upper part, but resistivity and velocity decreases in the deeper part of the profile (SYN3). Velocity and resistivity values vary up to 50 % compared to the baseline model with generally higher magnitudes for the RST data. All three scenarios show a unique pattern of changes in ρ_s and v_p and should therefore in general be distinguishable by the combination of ERT and RST. By construction, the defined zones in the synthetic models have sharp edges and show big contrasts to their neighbouring zones with different geophysical characteristics.

4.1.2 Inverted synthetic models

Figure 5 a,b show the inverted models of the synthetic data presented in Figure 4 as well as their relative changes with respect to the baseline model (Fig. 5c,d). Due to the standardly used regularisation constraints of the inversion (cf. Hauck and Vonder Mühll, 2003; Hilbich et al., 2009) all models represent a smoothed version of their counterparts in Figure 4, but the simulated processes are not always visible by looking at the ERT and RST tomograms alone. They first become visible in the analysis of the significant changes in ρ_s and v_p, seen in Fig. 5c and d. The spatial resolution of most features is weak, due to the coarse electrode/geophone spacing of 4.5 m. However, the unique pattern of resistivity/velocity changes identified in Figure 4 (marked by the blue, green and pink rectangles, respectively) is clearly visible also in the inverted tomograms. The thickness of the layers with water saturation (SYN2 & SYN3) and ice loss (SYN4) is hereby strongly overestimated (by a factor 2-3). Moreover, the depth at which ice loss is detected in SYN4 is too shallow, especially in the ERT tomogram. The vertical pattern of the preferential flow paths is clearly visible in the velocity changes and to a lesser amount in the resistivity changes, but preferential flow paths below the ice body are poorly resolved. From Fig. 5c and d it is also visible that inversion artifacts are produced with both methods for almost all scenarios.

Another important feature of the inverted data sets is the general underestimation of the thaw depth of 5 metres by the ERT method (~2-3 m in Fig. 5a). This is partly due to the coarse electrode spacing but also due to the very strong resistivity contrast between active layer and ice-rich permafrost, causing inversion artifacts.

4.2 Analysis of 4PM results

4.2.1 Synthetic models

Figure 6 shows the calculated 4PM results for the three theoretical scenarios of Figure 5 a,b. The simulated water-, ice- and air content patterns are correctly reproduced by the 4PM, as should be expected because the 4PM uses the resistivity and velocity values of Table 1, which were also used to transfer the synthetic models to their respective ERT and RST counterparts. However, to achieve this good match two specific constraints were necessary:

a) Low ρ_s and v_p values at the surface often cause erroneous values in the 4PM. In mountain permafrost studies these low values at the surface correspond to the thaw depth (ice content = 0), which can therefore be estimated by the so-

The Cryosphere Discuss., doi:10.5194/tc-2016-229, 2016
Manuscript under review for journal The Cryosphere
Published: 1 November 2016

called 3-phase model (3PM, cf. Pellet et al., 2016). In such cases the ice content is automatically set to 0 % to better constrain the calculation of water and air contents.

b) A realistic porosity model including the bedrock topography is crucial for a modelling of realistic ice contents (see uppermost panel in Figure 6 a). A combined analysis of ρ_s and v_p and the 3PM-derived porosity distribution (assuming an ice content = 0) allows to delineate the bedrock topography: in cases of high resistivities and velocities >> 3500 m/s at greater depth a low porosity (corresponding to bedrock) can be assumed.

Figure 7 confirms that also the 4PM-calculated changes in ice-, water- and air contents (relative to the baseline model) perfectly represent all simulated processes. Note, that the horizontal preferential flow below the ice core (SYN3) is small and almost invisible in Figure 7b, but correctly modelled, as it takes place in low-porosity bedrock (cf. porosity model in Figure 6).

4.2.2 Inverted synthetic models

When applying the 4PM not to the synthetic models, but to the inverted data, i.e. after one complete forward-inverse cycle, the uncertainties with respect to measurement geometry and inversion (cf. Fig. 6) and with respect to the formulation of the 4PM become apparent (Figure 8). Most simulated processes are reproduced, but with weaker spatial resolution and smaller amplitudes. Best results are obtained for SYN4, which unambiguously shows the ice loss, which is compensated by an increase in air content. However, there are considerable differences compared to the ideal case in Figure 7. First of all, the overall magnitude of changes is much lower (5-10 % as opposed to the correct value of 40 % in Fig. 7). In the SYN2 scenario the strong increase in water content, caused also by an overestimated thickness of the saturated layer in the resistivity inversion (Fig. 6), is partly compensated by an erroneous decrease in ice content. In general this means that detected ice losses in the 4PM could also originate from inversion artifacts (mainly in the ERT data) caused by strong resistivity contrasts, as e.g. in the SYN2 scenario (saturated flow above the ice body). In addition, the 5 % Gaussian noise produced a similar anomaly pattern on the right hand boundary of the tomogram which is also a pure inversion artefact.

The vertical preferential flow paths (SYN3) can roughly be delineated and the resulting pattern is similar (but smoothed) to the pattern observed in the synthetic 4PM experiment (Figure 7). The horizontal saturated layer below the ice body, however, produces a similar artefact as for the SYN2 experiment, with a too thick and too strong decrease in ice content that compensates a similar increase in water content. The signature of the patterns corresponds, with the exception of the ice content decrease in SYN2, however to the synthetic model experiments shown in Figure 7.

The Cryosphere Discuss., doi:10.5194/tc-2016-229, 2016
Manuscript under review for journal The Cryosphere
Published: 1 November 2016

4.3 Analysis of inverted field data

4.3.1 Geophysical monitoring

The synthetic modelling results of the previous sections have indicated that the three permafrost and hydrology related processes can be detected on rock glaciers with a combination of ERT and RST although uncertainties may arise during inversion, especially when coarse sensor spacings are used (4.5 m in the present case), or when the features of interest are located at relatively great depth. In this section the approach is now tested on real field data from the Becs-de-Besson rock glacier.

Figure 9 shows the ERT and RST inversion results for three measurement dates beginning and end of summer 2012 and 2013. The consistency of all tomograms is clearly seen with a strong contrast between active layer (lower resistivity and velocity values) and ice body (higher resistivity and velocity values). Lateral variability exists, both in the ERT as well as RST data, corresponding to the lateral variability of the ice core (see detailed interpretation in section 3.3). Temporal changes are supposed to be caused solely by water infiltration and seasonal ice melt processes. Note, that similar to Figure 5 a and b the thaw depth is significantly smaller in the ERT results than in RST results (for July 2012 ~2-3 m in the ERT and ~4-5 m in the RST data). The actual thaw depth is therefore assumed to be better resolved in the RST data, i.e. around 4 m.

Figure 11 shows the percentage resistivity and velocity changes for a one-year period (beginning of summer measurements, upper panel) and over a summer season in 2013 (lower panel). It is seen that the percentage P-wave velocity changes are much larger than corresponding resistivity changes, highlighting again the general usefulness of RST monitoring in permafrost applications (Hilbich, 2010; Dräbing, 2016). Resistivity generally decreased between July 2012 and July 2013 with a predominant increase in P-wave velocities with largest changes in the downslope part near the rock glacier tongue (Fig. 10a). This change pattern corresponds to the SYN2 experiment in Fig. 8 indicative for an increase in water content in the active layer. Increasing water content in an unfrozen blocky layer would lead to a resistivity decrease (water having a lower electrical resistivity than air, rock or ice, cf. Tables 1 and 2) and a P-wave velocity increase, as the P-wave velocity of water is higher than that of air (1500 m/s versus 330 m/s, cf. Table 2). However, the seismic results (Fig. 10b upper panel) show also regions with decreasing P-wave velocity (which partly correspond to zones with unchanging or slightly increasing resistivity) indicating that there are also regions with decreasing water content present, especially in the upslope part of the rock glacier.

For the seasonal evolution during the year 2013 (Fig. 10, lower panel) the generally decreasing resistivity and velocity patterns correspond to the SYN4 experiment (Figure 8 right panel). These results visualise the thawing of the active layer between the two measurement dates at the end of July and end of September, which corresponds roughly to the snow-free period. Borehole temperatures from the nearby PERMOS station Lapires BH98/01 at similar altitude indicate a propagation of the thawing front from about 1.0 m to 4.9 m between 25 July and 27 September 2013 (PERMOS, 2016). The contemporaneous decrease of resistivity and velocity during that period is therefore indicative for seasonal ice loss in the active layer and corresponds to the process described in the synthetic model experiment SYN4, albeit at shallower depth.

The Cryosphere Discuss., doi:10.5194/tc-2016-229, 2016
Manuscript under review for journal The Cryosphere
Published: 1 November 2016

Similar to the conclusions drawn from the synthetic experiments (Figure 7 c and d), resistivity changes occur at shallower depths as velocity changes, but can be assumed to be caused by the same process (i.e. active layer thawing). No vertical structures are observed in Fig. 10, hence there are no indications of vertical preferential flow through the ice core.

4.3.2 4PM

Finally, Figure 11 shows the 4PM results for the two periods shown in Figure 10. Now, the processes but also the uncertainties described above can be analysed in more detail. The seasonal ice loss due to the advance of the thawing front during summer is clearly seen in Fig. 11b with a calculated ice content loss by 10-15 Vol.%. This ice content loss is compensated by an increase in air content (drying of the subsurface), especially in the central and upper part of the profile. Water content changes are small indicating a predominantly run-off of the melt water, except for a small increase on top of the presumed ice layer in the lower part of the profile. Lateral variability is high which might be due to the large heterogeneity of the rock glacier or due to the small-scale noise in the respective measurements, which can be amplified during inversion (e.g. Hauck et al., 2003). As the resistivity contrast in the downslope part of the field data is much smaller than in the synthetic data (comparing Figure 9 left panel and Figure 5 a), the inversion artifacts are assumed to be weaker or non-existent, i.e. the spatial dimensions of the changes in ice, water and air contents are assumed to be more realistic. Note that the overall changes of 10-15 % are relatively small compared to the synthetic experiments.

The inter-annual changes between 2012 and 2013 (Fig. 11a) produce a more complex pattern in the 4PM results. Ice content changes in the uppermost ~5 m (corresponding to the active layer) are predominantly negative, and positive below. Compensation is calculated mainly through increased (upper part) and decreased (lower part) air contents, but also a slight water content increase at the top of the ice body. The latter could be indicative for a change in saturation conditions in the active layer as hypothesized in the previous section.

It has to be noted though that the compensation between ice and air with a residual change in water content may have two reasons, one being process-based the other purely numerical: (a) due to the coarse grained material and the slope of the rock glacier, seasonally or inter-annually melting ice would rather result in quick infiltration and run-off on top of the ice-layer – ice loss would therefore lead to an increase in air content, but not an increase in water content; (b) the 4PM model formulation and the strong dependence of resistivity on water content (as opposed to ice, rock and air content, which are all considered as electrical isolators) can lead to a tendency of compensating effects between air and ice contents with independent determination of water content (cf. the structure of Eq. (1)-(3) and a thorough sensitivity analysis in Hauck et al 2011).

5. Discussion

The Cryosphere Discuss., doi:10.5194/tc-2016-229, 2016
Manuscript under review for journal The Cryosphere
Published: 1 November 2016

The synthetic modelling results presented above are very promising and lead the way to a geophysical monitoring of ice degradation and hydrologic processes within rock glaciers (or other coarse-grained permafrost material), although several limitations have to be faced. In order to distinguish between limitations caused by the inversion process and those caused by the 4PM model formulation, the results of inverted synthetic data and not inverted ("true") synthetic data are discussed separately.

4PM modelling of the true synthetic data show almost perfect results for the three different processes (Figure 6 and Figure 7), however, it has to be noted that a realistic porosity model is necessary to obtain realistic ice contents from the 4PM (cf. Hauck et al., 2011; Pellet et al., 2016). If no additional data are available (e.g. boreholes) it is crucial to approximate the bedrock topography of the rock glacier using a 3-phase model (3PM). Based on the assumption that no ice is present, the 3PM determines the porosity distribution, and bedrock can be identified from low-porosity zones with intermediate resistivities (e.g. a few 1000 Ωm) and high P-wave velocities (>> 3500 m/s) (Pellet et al., 2016). From this information the bedrock topography can be delineated and included in the porosity model of the 4PM (Figure 6). It has to be noted that the results of Figure 6 and Figure 7 describe the ideal case, where some often unknown input parameters for the 4PM were prescribed (e.g. the P-wave velocity of the rock material and the pore water resistivity) by using the same values as used for the construction of the synthetic models. This is not always the case in real applications.

All in all, vertical structures of increasing water content with respect to the baseline model are resolved well and at high resolution. The horizontal layer beneath the ice core in SYN3 is difficult to distinguish as 4PM-calculated water content changes are very small. This was expected, as changes in water content are predominantly seen in the ERT results, but an ice core acts as electrical isolator strongly decreasing the sensitivity of the method underneath. In addition, detection of a shallow water layer beneath an ice core poses also problems to RST, as seismic velocities would decrease with depth in this case and are therefore difficult to detect by refraction seismics (cf. Hilbich, 2010).

Largest errors are introduced by horizontally saturated layers (such as in SYN2) which are overestimated in thickness due to inversion artefacts, which in consequence lead to an erroneous decrease in ice content. This results in false ice loss detection in this scenario. In contrast, the true ice loss scenario in SYN4 is reproduced correctly, with a slight underestimation of the decreased ice content, and a correct resulting increase in air content in the part of the tomogram concerned. In spite of the limitations described above, most processes still can be detected in the 4PM results.

The spatial resolution of the 4PM calculations for the inverted synthetic data is much lower than for the true non-inverted synthetic data, and, as a consequence, the magnitude of changes is underestimated in the former experiments (cf. Figs. 7 and 8). This is on the one hand caused by the smoothing effect of the inversion process. In the absence of a-priori information, such as borehole data, standard inversion algorithms like the robust L1-Newton-Gauss used in this study have to apply smoothing constraints as regularisation due to the underdetermined nature of the inversion problem (e.g. Loke and Barker, 1995). On the other hand the low resolution and underestimated magnitude of change are due to the coarse sensor geometry, which was by intention chosen to be identical with the field data to simulate real field conditions. The sensor spacing of 4.5 m for the monitoring at Bec-de-Bosson is comparable to many other field sites in permafrost geophysics, where the profile

The Cryosphere Discuss., doi:10.5194/tc-2016-229, 2016
Manuscript under review for journal The Cryosphere
Published: 1 November 2016

length (ideally covering the entire landform) and the investigation depth (reaching the base of the landform) have similar high priority as spatial resolution. The results of this study therefore emphasise that interpretation of geophysical data and 4PM results could significantly be improved by using an increased spatial resolution of the sensor geometry, i.e. smaller electrode/geophone spacings.

Assuming that the small magnitudes of changes observed in our field data (Fig. 10) correspond to the poorly resolved changes in our synthetic experiments which originate from much stronger magnitudes, our results strongly suggest that observed processes are expected to be (i) much more pronounced in reality, but with (ii) smaller spatial dimension than illustrated by the geophysical inversions and the 4PM. Further, a systematic difference in the resolution of the thaw depth was observed, with a significantly smaller thickness in the ERT data compared to the RST data (cf. Fig. 5 and Fig. 9). The different inversion characteristics (smoothing and sensitivity, e.g. Marescot et al., 2003; Maurer and Hauck, 2007; Hilbich et al., 2009; Hilbich, 2010) of ERT and RST and the geometry limitations described above lead hereby to an overall overestimation of the spatial extent of both, conductive and resistive anomalies in the inversion results.

In the current version of 4PM, and for a completely prescribed porosity model, water content is only determined through Eq. (1) and not corrected by the RST data. Pellet et al. 2016 have shown that this can be improved through coupled 3PM and 4PM simulations, as well as near-surface calibration of the 4PM by measured soil moisture values. Future work should also explore the possibility of using alternative formulations of the resistivity mixing rule, that takes into account the resistivity of the rock material (Python, 2015). Finally, using alternative ERT inversion algorithms may also improve the delineation of sharply limited horizontal features.

The analysis of the results from the inverted synthetic data illustrates the difficulties for the interpretation of 4PM calculations of real field data. Inversion artefacts which are transferred to the 4PM may lead to false interpretations of the subsurface composition and the underlying processes (like degradation of ice cores or the existence of saturated layers). In combination with higher measurement errors in permafrost environments (up to 20 % instead of the 5 % used in the synthetic experiments, see e.g. Rosset et al., 2013) and only little a-priori information about the real subsurface structures, an interpretation of 4PM results can be much more complex and difficult.

However, the results of this study also demonstrate that interpretation of geophysical tomograms can be significantly facilitated through 4PM-based geophysical monitoring compared to a detailed interpretation of single tomograms because small-scale anomalies and processes are hardly resolvable from visual inspection of a tomogram alone (cf. Figure 5a and b).

6. Conclusion

We presented a detailed study about the resolution capacity of standard geophysical monitoring methods for the detection and analysis of ice- and water content changes in the context of mountain permafrost evolution. The study is based on synthetic and field data and analyses the individual performance of Electrical Resistivity Tomography (ERT) and Refraction Seismic Tomography (RST) inversions as well as their combined analysis within the so-called 4-phase model (4PM). Modelling and field results are shown for ground ice and water saturation changes in a rock glacier in the Western Swiss

Alps. Hereby, three scenarios were analysed: (i) development of a saturated layer on top of the ice core, (ii) preferential flow within the active layer and permafrost and (iii) ground ice loss, i.e. permafrost degradation. Key results of this study include:

- Our approach including complete forward-inverse cycles of synthetic data for the 4PM proved to be useful for estimating its resolution capacity regarding typical permafrost evolution scenarios. Limitations arising from the individual inversion as well as from the coupled approach with the 4PM can be distinguished.
- In general, monitoring adds information over singular surveys, as not only physical processes can be assessed, but also the negative impact of singular, and geometry induced inversion artifacts tend to be diminished. This is especially the case when using the combined analysis within the 4PM.
- the 4PM is able to reproduce the true, that is not-inverted, synthetic model scenarios almost perfectly – inaccuracies in the final 4PM results of the inverted scenarios stem rather from the individual inversion themselves. Inversion artifacts from the individual surveys are transported into 4PM analysis and lead to potential misinterpretation (such as wrongly detected ice loss in the synthetic case of the development of a saturated water layer on top of the ice core).
- For all geophysical monitoring with the 4PM a suitable porosity model is of great importance. Because porosity stays constant with time small errors in the porosity model will have only small impacts in a 4PM monitoring context.
- Apart from limitations stemming from coarse sensor geometry (4.5 m in our study) vertical structures can be resolved well, whereas the dimensions of saturated areas are overestimated by ERT and are more reliably determined from RST. Ice loss is well detectable with the 4PM, showing that the model is a valuable tool for geophysical monitoring of rock glaciers in the context of permafrost degradation.
- Due to the smoothing effect of most inversion algorithms, magnitudes of changes are often underestimated within the 4PM. Using different inversion algorithms with less smoothing should improve the magnitude of changes, but can be more susceptible for inversion artifacts.
- In applying the approach and findings of the synthetic model experiments, the monitoring field data from Bec-de-Bosson rock glacier showed heterogeneous saturation changes in the thaw layer between July 2012 and 2013, and seasonal propagation of the thaw layer (seasonal ice melt) between July and September 2013.
- However, for a detailed analysis of hydrological processes on field-scale rock glaciers, the sensor spacing of 4.5 m is too coarse and should be decreased. In its present configuration, larger changes in the hydrological system can be detected, but small scale variation of preferential flow is not yet detectable.

Acknowledgements

This study was conducted within the SNF-Sinergia project TEMPS financed by the Swiss National Science Foundation (project n° CRSII2 136279) and the authors would like to thank all colleagues within the project for their valuable input during meetings and conferences. We would like especially to thank Dr. B. Staub for his support regarding the fieldwork at Bec-de-Bosson rock glacier. Support from the PERMOS network (Permafrost Monitoring Switzerland) is thankfully acknowledged.

References

Archie, G. E.: The electrical resistivity log as an aid in determining some reservoir characteristics, Transactions of the AIME, 146, 54–62, 1942.

Arenson, L., Hauck, C., Hilbich, C., Seward, L., Yamamoto, Y. and Springman, S.: Sub-surface heterogeneities in the Murtèl-Corvatsch rock glacier, Switzerland, Geo2010, 6th Canadian Permafrost Conference, Calgary, Canada, 1494–1500, 2010.

Barsch, D.: Rockglaciers - Indicators for the Present and Former Geoecology in High Mountain Environments, 16, Springer, Heidelberg, 1996.

Buchli, T., K. Merz, X. Zhou, W. Kinzelbach, and Springman, S. M.:. Characterization and Monitoring of the Furggwanghorn Rock Glacier, Turtmann Valley, Switzerland: Results from 2010 to 2012. Vadose Zone J. 12. doi:10.2136/vzj2012.0067, 2013.

Delaloye, R.: Contribution à l'étude du pergélisol de montagne en zone marginale., PhD Thesis, University Fribourg, Fribourg., 2004.

Delaloye, R. and Perruchoud, D.: Surveying the (seasonal) variations in rock glacier activity using GPS technique (western Swiss Alps), Terra Nostra, 99–100, 2005.

Delaloye, R., Perruchoud, E., Avian, M., Kaufmann, V., Bodin, X., Hausmann, H., Ikeda, A., Kääb, A., Kellerer-Pirklbauer, A., Krainer, K., Lambiel, C., Mihajlovic, D., Staub, B., Roer, I., and Thibert, E.: Recent Interannual Variations of Rock Glacier Creep in the European Alps, in: Ninth International Conference on Permafrost, Fairbanks, Alaska, United States, 343–348, 2008.

Dräbing, D.: Application of refraction seismics in alpine permafrost studies: A review, Earth-Science Reviews, 155, 136–152, 2016.

Duguay, M. A., A. Edmunds, L. U. Arenson, and Wainstein, P. A.: Quantifying the significance of the hydrological contribution of a rock glacier – A review, GeoQuebec 2015 - 68th Canadian geotechnical conference and 7th Canadian permafrost conference, Quebec, Canada, Sept. 20-23, 2015.

Fortier, R., LeBlanc, A.-M., Allard, M., Buteau, S., and Calmels, F.: Internal structure and conditions of permafrost mounds at Umiujaq in Nunavik, Canada, inferred from field investigation and electrical resistivity tomography, Canadian Journal of Earth Sciences, 45, 367–387, 2008.

Gardaz, J.-M.: Permafrost prospecting. Periglacial and rock glacier hydrology in mountain areas : case studies in the Valais Alps, Switzerland, PhD thesis, Univ. Press, Fribourg, Switzerland, 1999.

Haeberli, W., Hallet, B., Arenson, L., Elconin, R., Humlum, O., Kääb, A., Kaufmann, V., Ladanyi, B., Matsuoka, N., Springman, S., and Vonder Mühll, D.: Permafrost creep and rock glacier dynamics, Permafrost Periglac. Process., 17, 189–214, doi:10.1002/ppp.561, 2006.

Hauck, C.: New Concepts in Geophysical Surveying and Data Interpretation for Permafrost Terrain, Permafrost and Periglac. Process., 24, 131–137, doi:10.1002/ppp.1774, 2013.

Hauck, C., Böttcher, M., and Maurer, H.: A new model for estimating subsurface ice content based on combined electrical and seismic data sets, The Cryosphere, 5, 453–468, 2011.

Hauck, C. and Kneisel, C. (Eds.): Applied Geophysics in Periglacial Environments, Cambridge University Press, Cambridge, 2008.

Hauck, C. and Vonder Mühll, D.: Inversion and interpretation of two-dimensional geoelectrical measurements for detecting permafrost in mountainous regions, Permafrost and Periglacial Processes, 14, 305–318, 2003.

Hausmann, H., Krainer, K., Brückl, E., and Mostler, W.: Internal structure and ice content of Reichenkar rock glacier (Stubai Alps, Austria) assessed by geophysical investigations, Permafrost and Periglacial Processes, 18, 351–367, 2007.

Hilbich, C.: Time-lapse refraction seismic tomography for the detection of ground ice degradation, The Cryosphere, 4, 243–259, doi:10.5194/tc-4-243-2010, 2010.

Hilbich, C., Fuss, C., and Hauck, C.: Automated Time-lapse ERT for Improved Process Analysis and Monitoring of Frozen Ground, Permafrost and Periglac. Process., 22, 306–319, doi:10.1002/ppp.732, 2011.

Hilbich, C., Hauck, C., Hoelzle, M., Scherler, M., Schudel, L., Völksch, I., Mühll, D. V., and Mäusbacher, R.: Monitoring mountain permafrost evolution using electrical resistivity tomography: A 7-year study of seasonal, annual, and long-term variations at Schilthorn, Swiss Alps, J. Geophys. Res., 113, 1–12, doi:10.1029/2007JF000799, 2008.

Hilbich, C., Marescot, L., Hauck, C., Loke, M. H., and Mäusbacher, R.: Applicability of electrical resistivity tomography monitoring to coarse blocky and ice-rich permafrost landforms, Permafrost and Periglacial Processes, 20, 269–284, 2009.

Humlum, O.: Active layer thermal regime at three rock glaciers in Greenland, Permafrost and Periglacial Processes, 8, 383–408, doi:10.1002/(SICI)1099-1530(199710/12)8:4<383:AID-PPP265>3.0.CO;2-V, 1997.

Ikeda, A., Matsuoka, N., and Kääb, A.: Fast deformation of perennially frozen debris in a warm rock glacier in the Swiss Alps: an effect of liquid water, Journal of Geophysical Research: Earth Surface, 113, 2008.

Jansen, F. and Hergarten, S.: Rock glacier dynamics: Stick-slip motion coupled to hydrology, Geophys. Res. Lett., 33, doi:10.1029/2006GL026134, 2006.

Kääb, A.: Remote Sensing of Mountain Glaciers and Permafrost Creep. Research Perspectives from Earth Observation Technologies and Geoinformatics, Schriftenreihe Physische Geographie, 48, Institute for Geography University Zurich, 2005.

Kellerer-Pirklbauer, A. and Kaufmann, V.: About the relationship between rock glacier velocity and climate parameters in central Austria, Austrian Journal of Earth Sciences, 105, 94–112, 2012.

Kneisel, C., Hauck, C., Fortier, R., and Moorman, B.: Advances in geophysical methods for permafrost investigations, Permafrost Periglac. Process., 19, 157–178, doi:10.1002/ppp.616, 2008.

Kneisel, C., Rödder, T., and Schwindt, D.: Frozen ground dynamics resolved by multi-year and yearround electrical resistivity monitoring at three alpine sites in the Swiss Alps, Near Surface Geophysics, 12, 117–132, 2014.

Knödel, K., Krummel, H., and Lange, G.: Handbuch zur Erkundung des Untergrundes von Deponien und Altlasten: Band 3: Geophysik, Springer-Verlag, 2013.

Kobierska, F., Jonas, T., Griessinger, N., Hauck, C., Huxol, S., and Bernasconi, S. M.: A multi-method field experiment to determine local groundwater flow in a glacier forefield, Hydrological Processes, 29, 817–827, 2015.

Krainer, K. and He, X.: Flow velocities of active rock glaciers in the Austrian Alps. Geografiska Annaler: Series A, Physical Geography, 88, 267–280. doi:10.1111/j.0435-3676.2006.00300.x, 2006.

Krainer, K. and Mostler, W.: Hydrology of active rock glaciers: examples from the Austrian Alps, Arctic, Antarctic, and Alpine Research, 142–149, 2002.

Krautblatter, M., Verleysdonk, S., Flores-Orozco, A., and Kemna, A.: Temperature-calibrated imaging of seasonal changes in permafrost rock walls by quantitative electrical resistivity tomography (Zugspitze, German/Austrian Alps), Journal of Geophysical Research: Earth Surface, 115, doi:10.1029/2008JF001209, 2010.

Langston, G., Bentley, L. R., Hayashi, M., McClymont, A., and Pidlisecky, A.: Internal structure and hydrological functions of an alpine proglacial moraine, Hydrological Processes, 25, 2967–2982, 2011.

Lehmann-Horn, J. A., Walbrecker, J.O., Hertrich, M., Langston, G., McClymont, A.F. and Green, A.G.: Imaging groundwater beneath a rugged proglacial moraine, Geophysics, 76: B165–B172, 2011.

Loke, M. H.: Res2DMOD, Geotomo, 2002.

Loke, M. H.: Res2DInv, Geotomo, 2015.

Loke, M. H. and Barker, R. D.: Least-squares deconvolution of apparent resistivity pseudosections, Geophysics, 60, 1682–1690, 1995.

Loke, M. H., Chambers, J. E., Rucker, D. F., Kuras, O., and Wilkinson, P. B.: Recent developments in the direct-current geoelectrical imaging method, Journal of Applied Geophysics, 95, 135–156, 2013.

Marescot, L., Loke, M. H., Chapellier, D., Delaloye, R., Lambiel, C., and Reynard, E.: Assessing reliability of 2D resistivity imaging in mountain permafrost studies using the depth of investigation index method, Near Surface Geophysics, 1, 57–67, 2003.

Mari, S., Scapozza, C., Pera, S. and Delaloye, R.: Prove di multitracciamento di ghiacciai rocciosi e ambienti periglaciali nel Vallon de Réchy (VS) e nella Valle di Sceru (TI), Bollettino della Società ticinese di scienze naturali, 101,13-20, 2013.

Maurer, H. and Hauck, C.: Geophysical imaging of alpine rock glaciers, Journal of Glaciology, 53, 110–120, 2007.

Merz, K., Maurer, H., Buchli, T., Horstmeyer, H., Green, A. G., and Springman, S. M.: Evaluation of Ground-Based and Helicopter Ground-Penetrating Radar Data Acquired Across an Alpine Rock Glacier, Permafrost and Periglacial Processes, 26, 13–27, 2015.

Monnier, S., Camerlynck, C., Rejiba, F., Kinnard, C., Feuillet, T., and Dhemaied, A.: Structure and genesis of the Thabor rock glacier (Northern French Alps) determined from morphological and ground-penetrating radar surveys, Geomorphology, 134, 269–279, 2011.

Monnier, S. and Kinnard, C.: Internal structure and composition of a rock glacier in the Andes (upper Choapa valley, Chile) using borehole information and ground-penetrating radar, Annals of Glaciology, 54, 61–72, 2013.

Pellet, C., Hilbich, C., Marmy, A., and Hauck, C.: Soil Moisture Data for the Validation of Permafrost Models Using Direct and Indirect Measurement Approaches at Three Alpine Sites, Frontiers in Earth Science, 3, 91, doi:10.3389/feart.2015.00091, 2016.

PERMOS: PERMOS Database. Swiss Permafrost Monitoring Network, Fribourg, Switzerland. DOI:10.13093/permos-2016-01, 2016.

Perruchoud, E. and Delaloye, R.: Short-term changes in surface velocities on the Becs-de-Bosson rock glacier (western Swiss Alps), Grazer Schriften der Geographie und Raumforschung, 43, 131-136, 2007.

Python, S.: Technical improvement of the 4-phase model to better assess the ice, water and air content estimation in permafrost substrates, Master thesis, Université de Fribourg, Fribourg, 2015.

Rosset, E., Hilbich, C., Schneider, S., and Hauck, C.: Automatic filtering of ERT monitoring data in mountain permafrost, Near Surface Geophysics, 11, 423–433, 2013.

Sandmeier, K.-J.: ReflexW 7.5, Sandmeier, 2015.

Sawada, Y., Ishikawa, M., and Ono, Y.: Thermal regime of sporadic permafrost in a block slope on Mt. Nishi-Nupukaushinupuri, Hokkaido Island, Northern Japan, Geomorphology, 52, 121–130, doi:10.1016/S0169-555X(02)00252-0, 2003.

Scapozza, C., Gex, P., Lambiel, C. and Reynard, E.: Contribution of self-potential (SP) measurements in the study of alpine periglacial hydrology: examples from the southern Swiss Alps, In Proceedings of the 9th International Conference on Permafrost, Fairbanks, Alaska, Kane DL, Hinkel KM. (eds). Institute of Northern Engineering, University of Alaska Fairbanks: Fairbanks, Alaska, USA; 1583–1588, 2008.

Scherler, M., Hauck, C., Hoelzle, M., Stähli, M., and Völksch, I.: Meltwater infiltration into the frozen active layer at an alpine permafrost site, Permafrost and Periglacial Processes, 21, 325–334, 2010.

Schneider, S., Daengeli, S., Hauck, C., and Hoelzle, M.: A spatial and temporal analysis of different periglacial materials by using geoelectrical, seismic and borehole temperature data at Murtèl–Corvatsch, Upper Engadin, Swiss Alps, Geogr. Helv, 68, 265–280, 2013.

Schön, J. H.: Physical properties of rocks: Fundamentals and principles of petrophysics, Elsevier, 2015.

Scott, W. J., Sellmann, P., and Hunter, J. A.: Geophysics in the study of permafrost, Geotechnical and Environmental Geophysics, 1, 355–384, 1990.

Staub, B, and Delaloye, R: Using Near-Surface Ground Temperature Data to Derive Snow Insulation and Melt Indices for Mountain Permafrost Applications. Permafrost and Periglac. Process., doi: 10.1002/ppp.1890, 2016.

Supper, R., Ottowitz, D., Jochum, B., Roemer, A., Pfeiler, S., Kauer, S., and Ita, A.: Geoelectrical monitoring of frozen ground and permafrost in alpine areas: field studies and considerations towards an improved measuring technology, 2014.

Tenthorey, G.: Paysage géomorphologique du Haut-Val de Réchy (Valais, Suisse) et hydrologie liée aux glaciers rocheux, 1993.

Tenthorey, G.: Hydrologie liée aux glaciers rocheux, Haut-Val de Réchy (Nax, VS), Bulletin de la Murithienne, 97–116, 1994.

Timur, A.: Velocity of compressional waves in porous media at permafrost temperatures, Geophysics, 33, 584–595, 1968.

Voytek, E.B., Rushlow, C.R., Godsey, S.E. and Singha, K., Identifying hydrologic flowpaths on arctic hillslopes using electrical resistivity and self potential, Geophysics, 81(1), pp.WA225-WA232, 2016.

Wilkinson, P. B., Chambers, J. E., Meldrum, P. I., Gunn, D. A., Ogilvy, R. D., and Kuras, O.: Predicting the movements of permanently installed electrodes on an active landslide using time-lapse geoelectrical resistivity data only, Geophysical Journal International, 183, 543–556, 2010.

Wright, N., Hayashi, M., and Quinton, W. L.: Spatial and temporal variations in active layer thawing and their implication on runoff generation in peat-covered permafrost terrain, Water Resources Research, 45, 2009.

Zimmerman, R. W. and King, M. S.: The effect of the extent of freezing on seismic velocities in unconsolidated permafrost, Geophysics, 51, 1285–1290, 1986.

List of Figures:

Figure 1: Map and photograph of the Bec de Bosson rock glacier. The red line marks the position of the geophysical profiles. Map source: Swiss Federal Office of Topography swisstopo.

Figure 2: Overview of the work flow applied in this study. Hereby, □a denotes the apparent resistivity, □s the specific resistivity and vp the P-wave velocity.

Figure 3: Creation of synthetic models based on inverted field data of the Bec-de-Bosson rock glacier: (a) inverted ERT and RST tomograms of 25 July 2013 with superposition of interpreted zones, (b) simplified synthetic baseline model (SYN1) based on the interpretation in (a) and different scenarios of hydrological processes (SYN2 to SYN4).

Figure 4: Synthetic model scenarios for (a) ERT and b) RST, and percentage changes between (c) ρs and (d) vp of the three scenarios with respect to the baseline model

Figure 5: Inverted synthetic model sections of the synthetic model scenarios of Figure 4 for (a) ERT and (b) RST, and percentage changes between (c) ρs and (d) vp of the three scenarios with respect to the baseline model. Inverted synthetic model sections of the synthetic model scenarios of Figure 4 for (a) ERT and (b) RST, and percentage changes between (c) ρ_s and (d) v_p of the three scenarios with respect to the baseline model. The positions of the introduced changes between the different scenarios are indicated by black lines.

Figure 6: 4PM results for the synthetic model scenarios (cf Figure 4 a,b). The blue, green and pink rectangles correspond to the same rectangles in Figures 3, 5 and 6. The prescribed porosity model is shown in the uppermost panel.

Figure 7: 4PM calculated changes in volumetric fractions for the three scenarios relative to the baseline model.

Figure 8: Changes in volumetric fractions for the 3 scenarios as in Figure 7, but now for the inverted synthetic data.

Figure 9: Inverted geophysical monitoring data from the Bec-de-Bosson rock glacier for three measurement dates in 2012 and 2013.

Figure 10: Temporal changes in (a) resistivity and (b) P-wave velocity between the measurements shown in Figure 9. Upper panel: interannual between 21 July 2012 and 25 July 2013. Lower panel: seasonal between 25 July and 27 September 2013. The coloured rectangles correspond to the resistivity/velocity change patterns in the synthetic experiments (cf. Figures 5-9).

Figure 11: Changes in volumetric fractions for the 2 time intervals of inverted monitoring data of the Bec-de-Bosson rock glacier: (a) 1 year (July 2012 to July 2013), (b) 2 months (July 2013 to September 2013).

The Cryosphere Discuss., doi:10.5194/tc-2016-229, 2016
Manuscript under review for journal The Cryosphere
Published: 1 November 2016

Figures

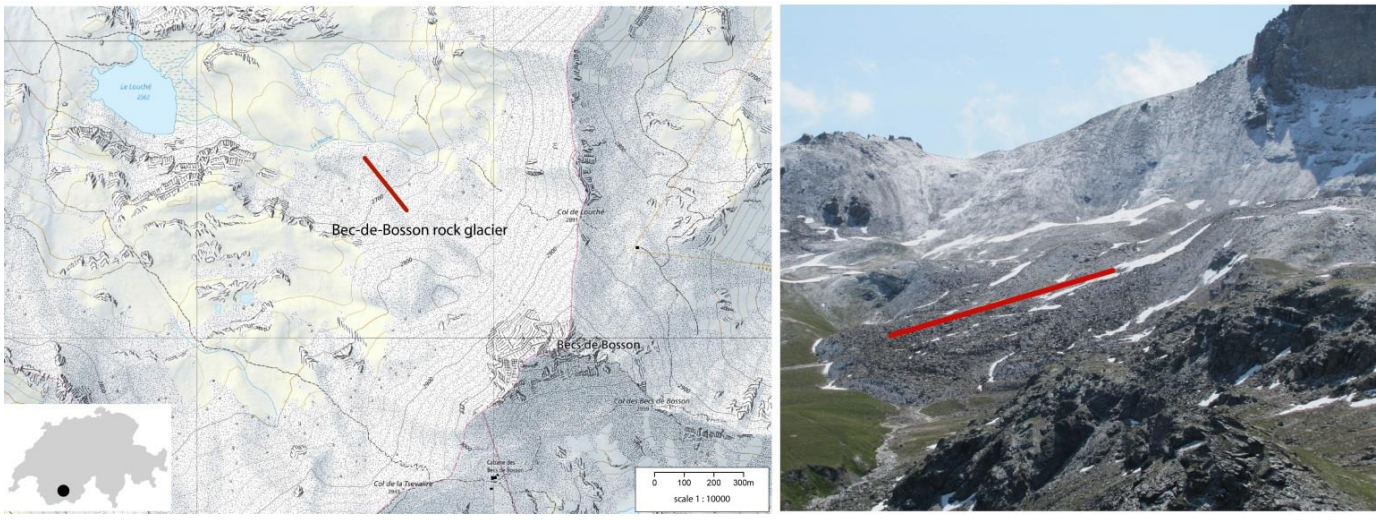

Figure 1: Map and photograph of the Bec de Bosson rock glacier. The red line marks the position of the geophysical profiles. Map source: Swiss Federal Office of Topography swisstopo.

The Cryosphere Discuss., doi:10.5194/tc-2016-229, 2016
Manuscript under review for journal The Cryosphere
Published: 1 November 2016

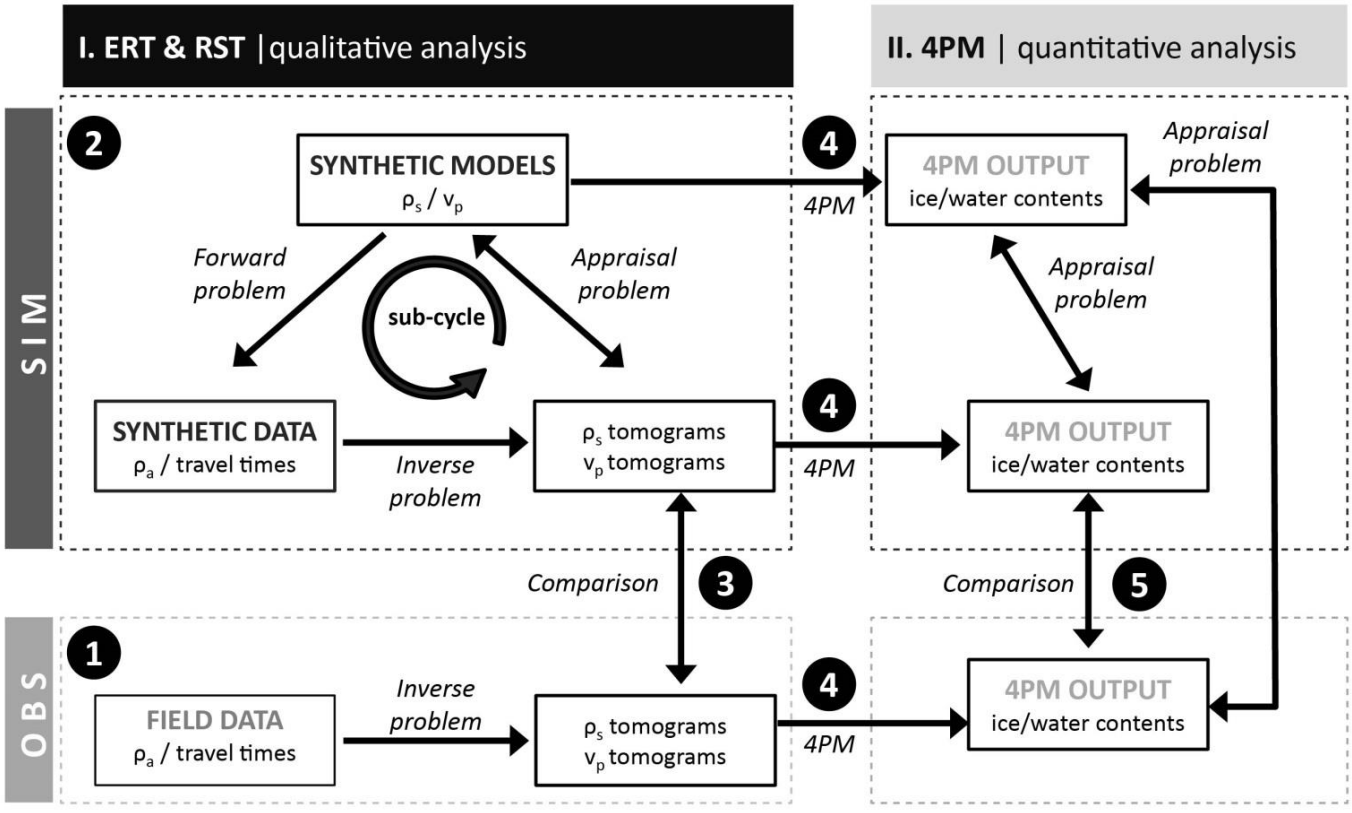

Figure 2: Overview of the work flow applied in this study. Hereby, ρ_a denotes the apparent resistivity, ρ_s the specific resistivity and v_p the P-wave velocity. Numbers 1 to 5 indicate the order of the individual steps.

The Cryosphere Discuss., doi:10.5194/tc-2016-229, 2016
Manuscript under review for journal The Cryosphere
Published: 1 November 2016

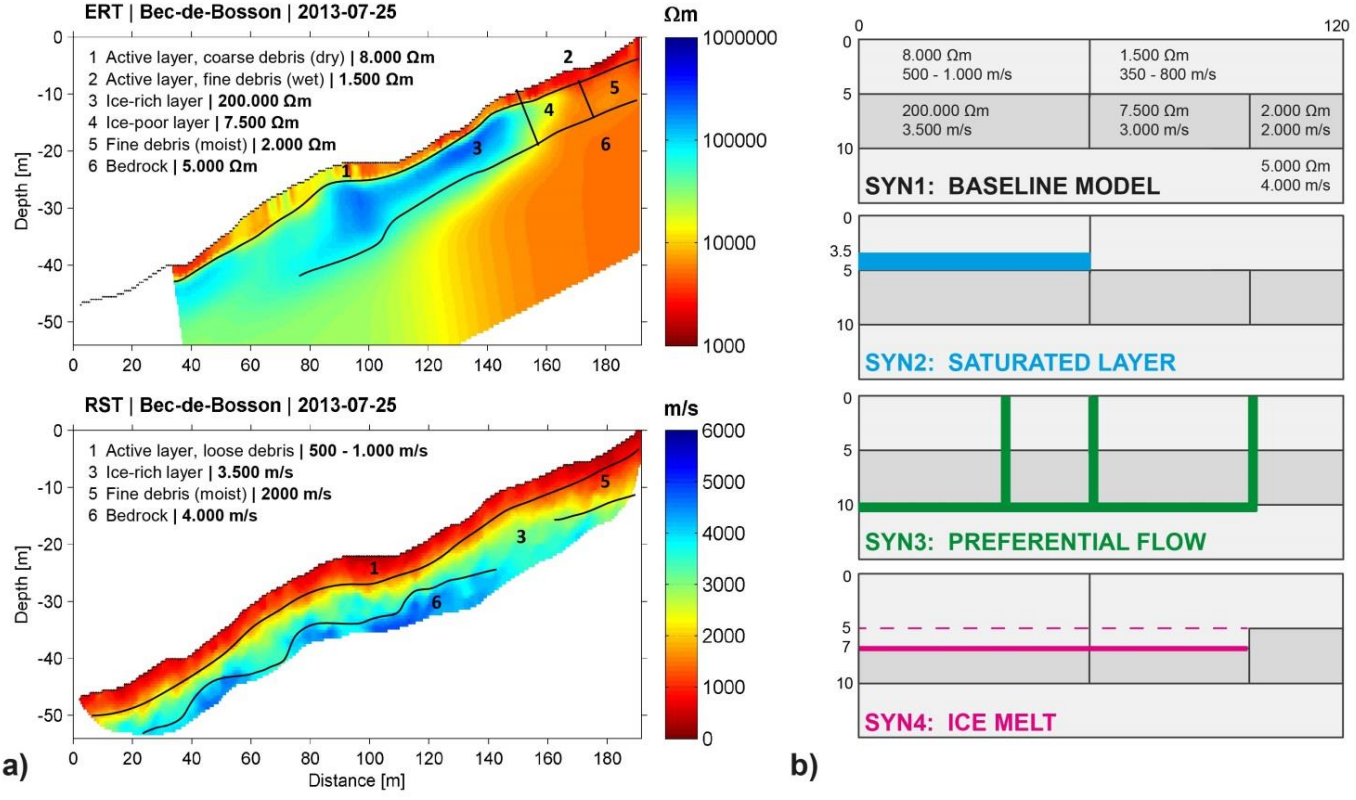

Figure 3: Creation of synthetic models based on inverted field data of the Bec-de-Bosson rock glacier: (a) inverted ERT and RST tomograms of 25 July 2013 with superposition of interpreted zones, (b) simplified synthetic baseline model (SYN1) based on the interpretation in (a) and different scenarios of hydrological processes (SYN2 to SYN4).

The Cryosphere Discuss., doi:10.5194/tc-2016-229, 2016
Manuscript under review for journal The Cryosphere
Published: 1 November 2016

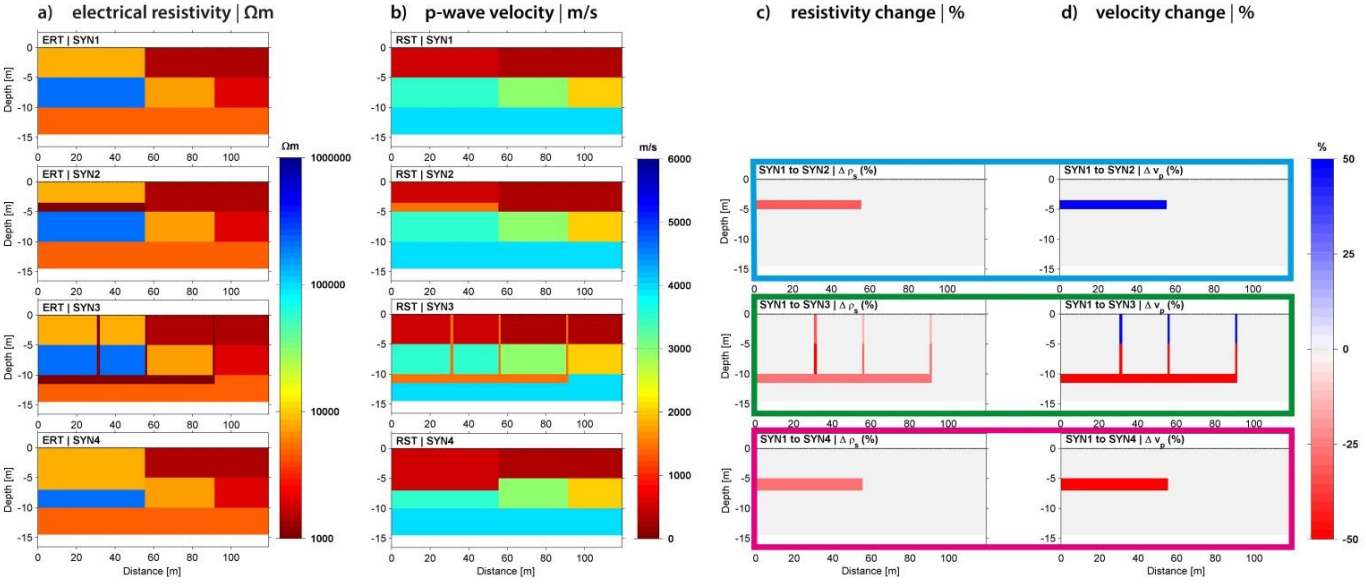

Figure 4: Synthetic model scenarios for (a) ERT and b) RST, and percentage changes between (c) ρ_s and (d) v_p of the three scenarios with respect to the baseline model.

The Cryosphere Discuss., doi:10.5194/tc-2016-229, 2016
Manuscript under review for journal The Cryosphere
Published: 1 November 2016

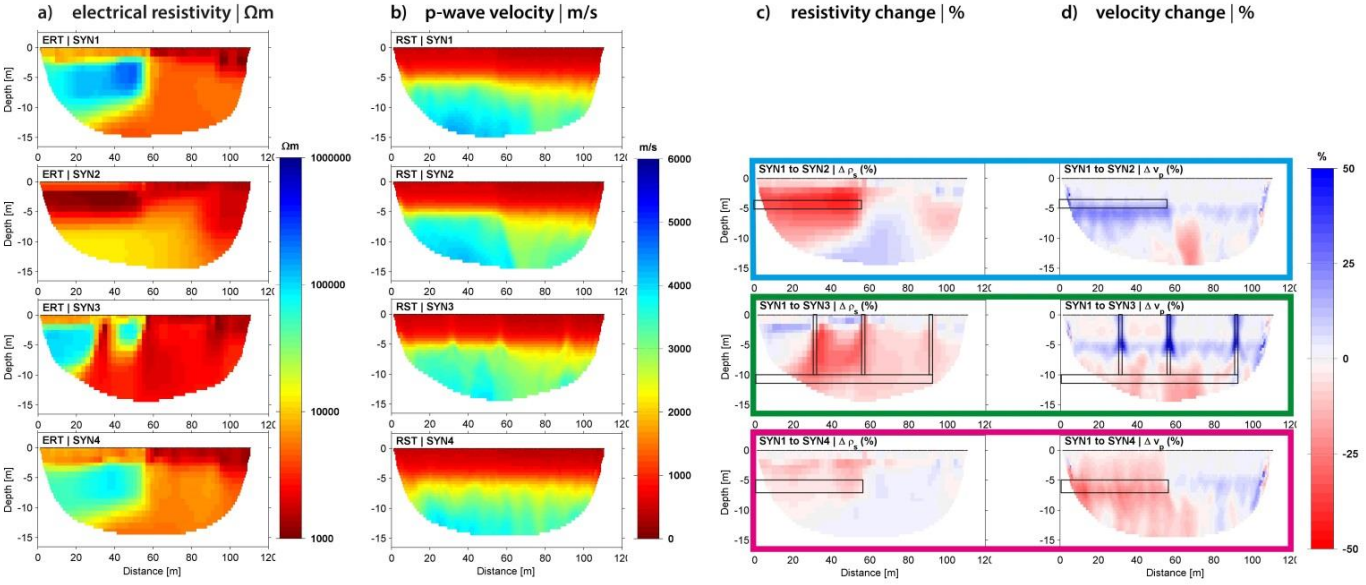

Figure 5: Inverted synthetic model sections of the synthetic model scenarios of Figure 4 for (a) ERT and (b) RST, and percentage changes between (c) ρ_s and (d) v_p of the three scenarios with respect to the baseline model. The positions of the introduced changes between the different scenarios are indicated by black lines.

The Cryosphere Discuss., doi:10.5194/tc-2016-229, 2016
Manuscript under review for journal The Cryosphere
Published: 1 November 2016

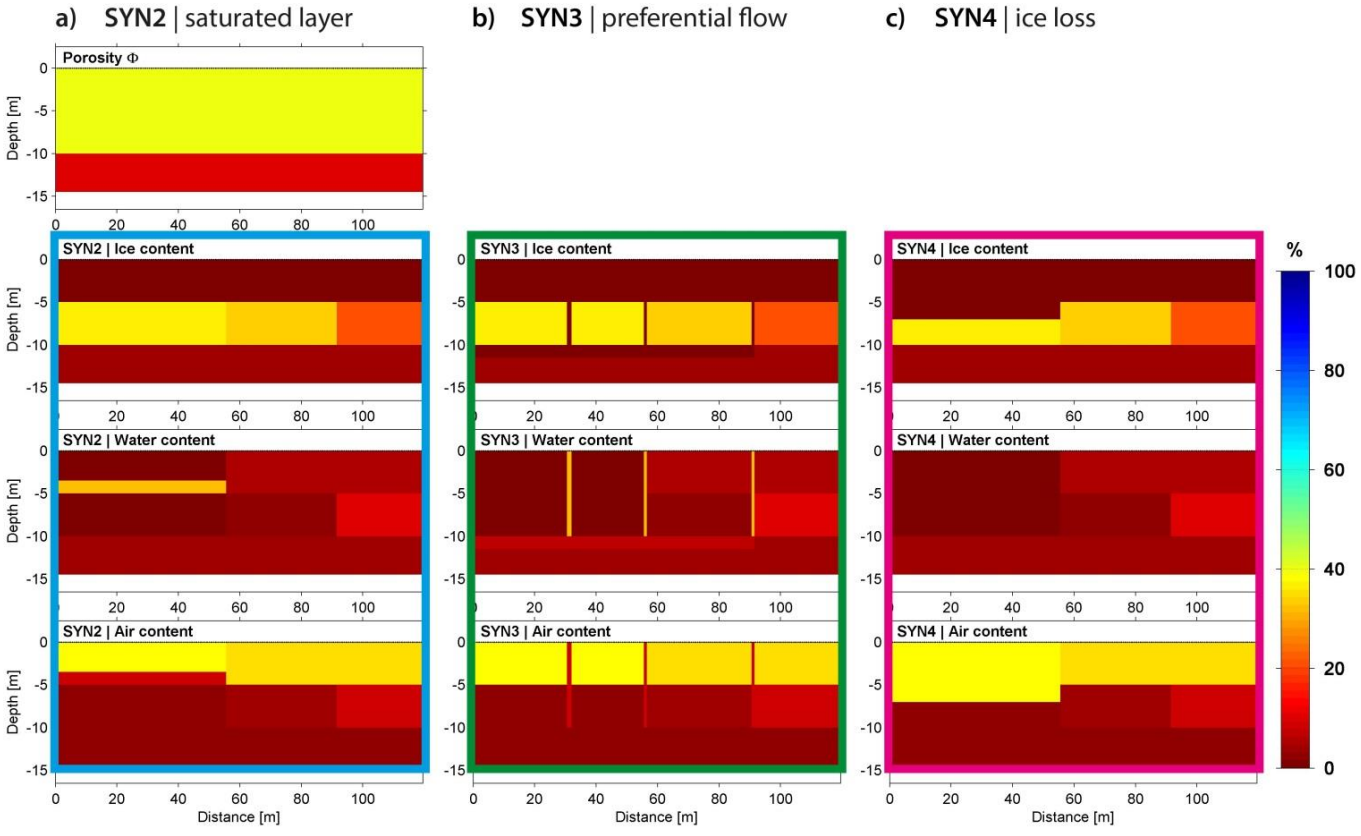

Figure 6: 4PM results for the synthetic model scenarios (cf Figure 4 a,b). The blue, green and pink rectangles correspond to the same rectangles in Figures 3, 5 and 6. The prescribed porosity model is shown in the uppermost panel.

The Cryosphere Discuss., doi:10.5194/tc-2016-229, 2016
Manuscript under review for journal The Cryosphere
Published: 1 November 2016

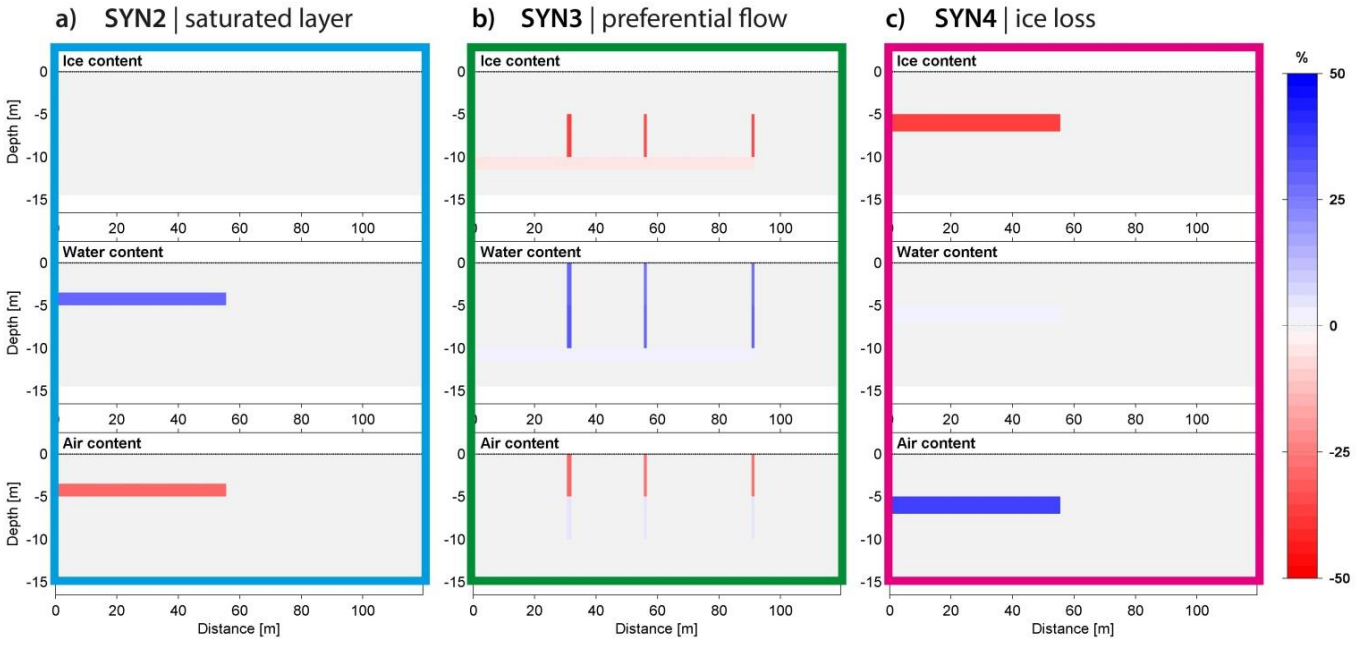

Figure 7: 4PM calculated changes in volumetric fractions for the three scenarios relative to the baseline model.

The Cryosphere Discuss., doi:10.5194/tc-2016-229, 2016
Manuscript under review for journal The Cryosphere
Published: 1 November 2016

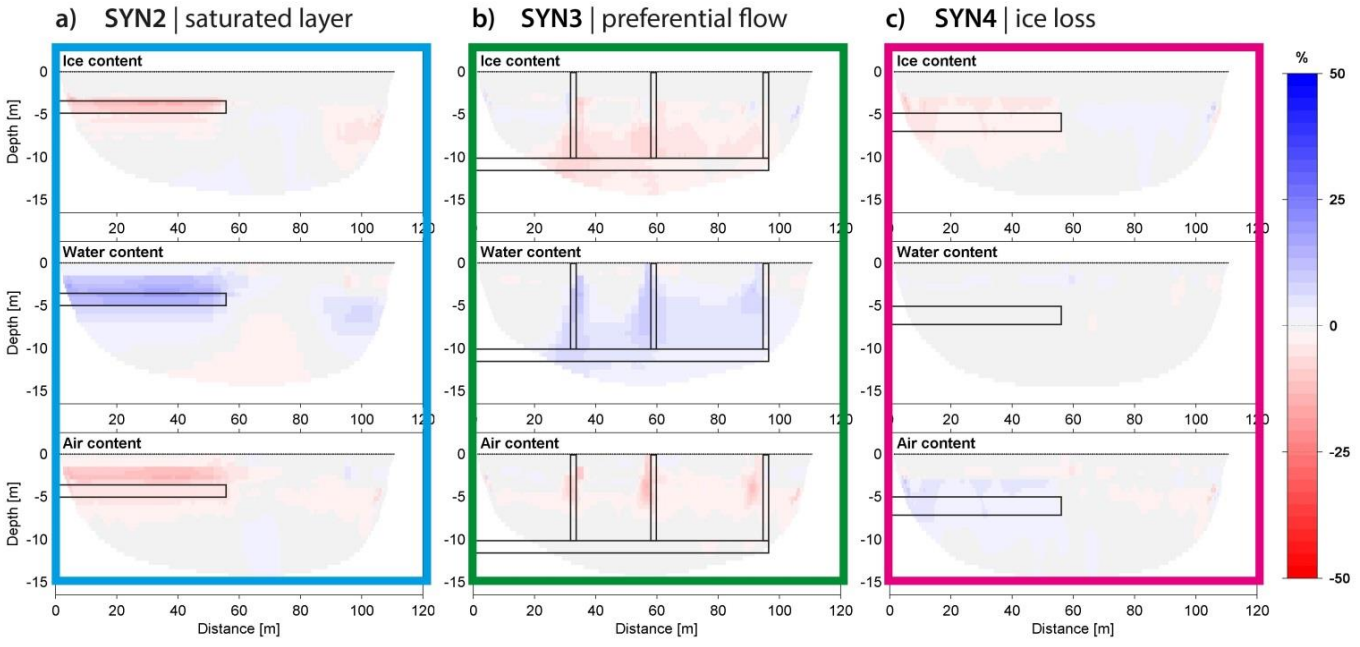

Figure 8: Changes in volumetric fractions for the 3 scenarios as in Figure 7, but now for the inverted synthetic data. The positions of the introduced changes between the different scenarios are indicated by black lines.

The Cryosphere Discuss., doi:10.5194/tc-2016-229, 2016
Manuscript under review for journal The Cryosphere
Published: 1 November 2016

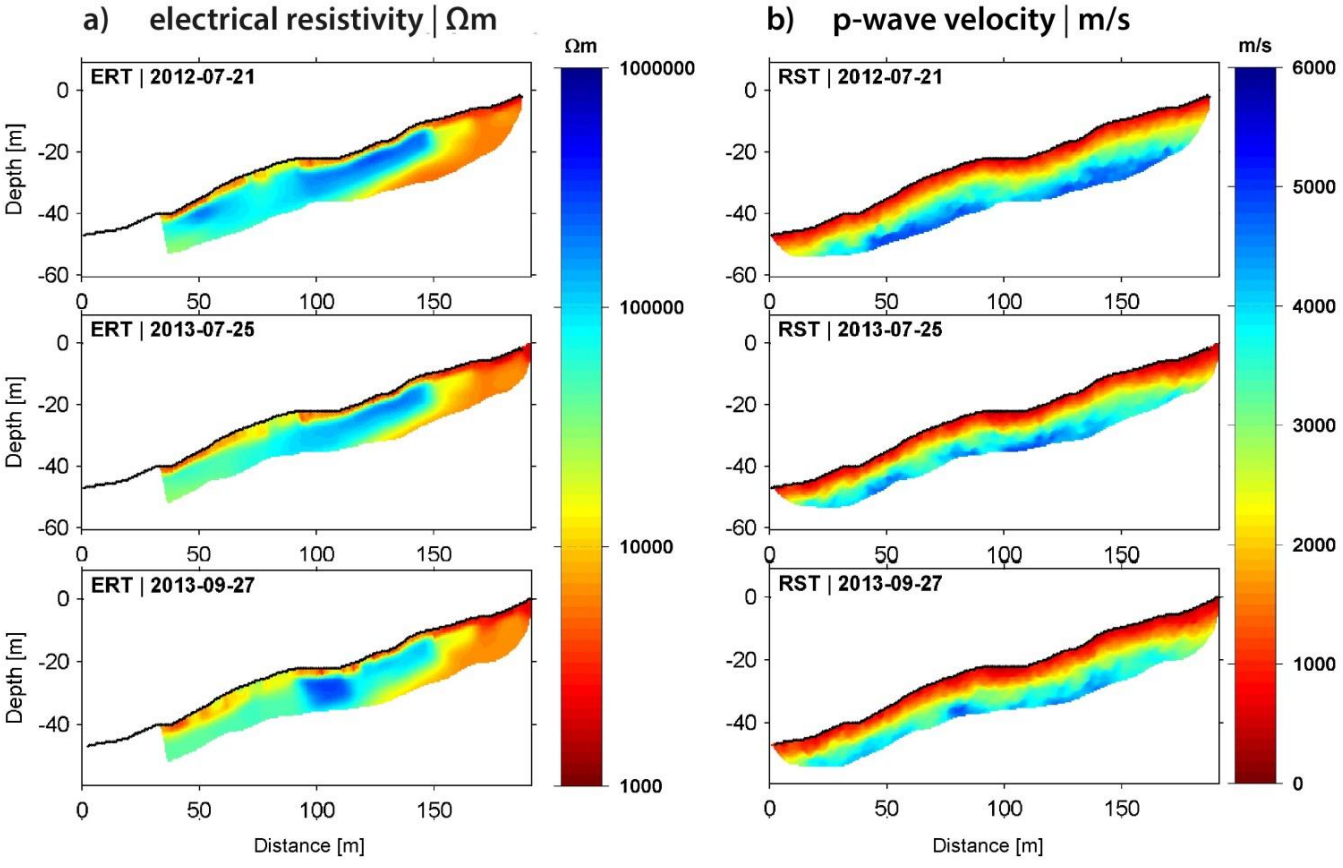

Figure 9: Inverted geophysical monitoring data from the Bec-de-Bosson rock glacier for three measurement dates in 2012 and 2013.

The Cryosphere Discuss., doi:10.5194/tc-2016-229, 2016
Manuscript under review for journal The Cryosphere
Published: 1 November 2016

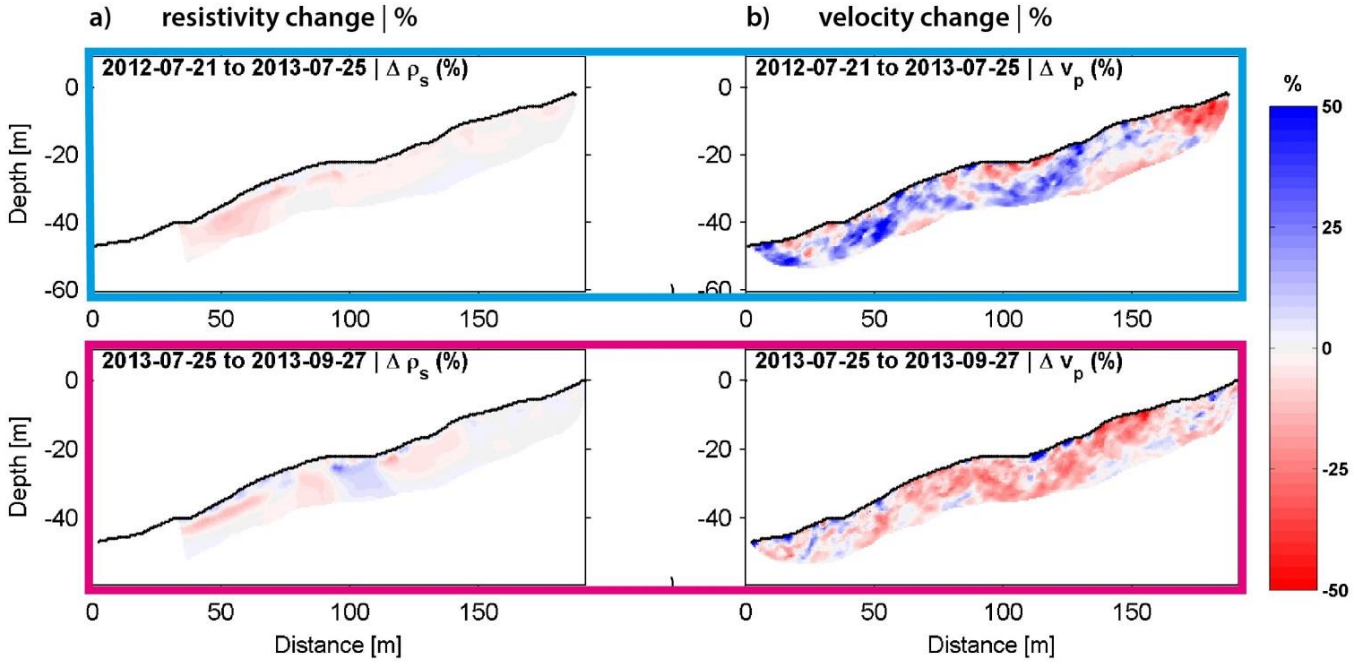

Figure 10: Temporal changes in (a) resistivity and (b) P-wave velocity between the measurements shown in Figure 9. Upper panel: interannual between 21 July 2012 and 25 July 2013. Lower panel: seasonal between 25 July and 27 September 2013. The coloured rectangles correspond to the resistivity/velocity change patterns in the synthetic experiments (cf. Figures 5-9).

The Cryosphere Discuss., doi:10.5194/tc-2016-229, 2016
Manuscript under review for journal The Cryosphere
Published: 1 November 2016

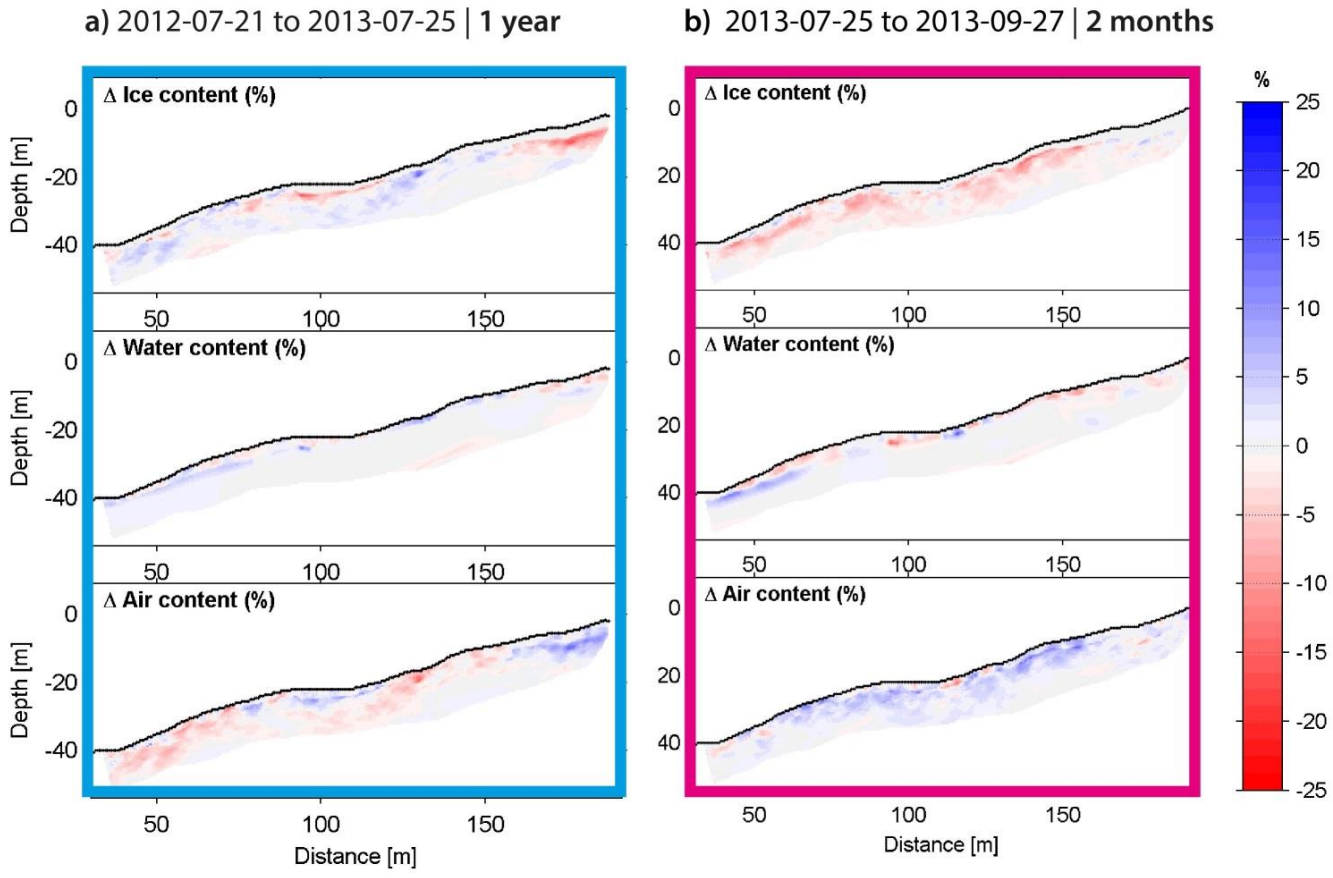

Figure 11: Changes in volumetric fractions for the 2 time intervals of inverted monitoring data of the Bec-de-Bosson rock glacier: (a) 1 year (July 2012 to July 2013), (b) 2 months (July 2013 to September 2013). Note the reduced range of the color scale.

The Cryosphere Discuss., doi:10.5194/tc-2016-229, 2016
Manuscript under review for journal The Cryosphere
Published: 1 November 2016

Table 1: Geophysical properties used in synthetic reference models. The values have been taken from literature (Barsch et al. 1996, Hauck & Kneisel 2008, Hilbich et al. 2009 and references therein) and adapted to match the inverted field data in an optimal way.

material	ρ_w	v_p
Unfrozen sediment (moist – dry)	3500 - 10000 Ωm	330 – 650 m/s
Ice-rich permafrost	200 000– 2 000 000 Ωm	3500 m/s
Ice-poor permafrost	200 000 Ωm	3300 m/s
Pore water ~~(in sediment)~~	100-500 Ωm	1500 m/s
Bedrock	3000 Ωm	6000 m/s

The Cryosphere Discuss., doi:10.5194/tc-2016-229, 2016
Manuscript under review for journal The Cryosphere
Published: 1 November 2016

Table 2: Overview over the values attributed to the free parameters in the 3 equations of the 4PM in this study.

Parameter	Value
V_w	1500 [m/s]
V_a	330 [m/s]
V_i	3500 [m/s]
V_r	6000 [m/s]
a	2
n	1
m	1
Φ_{ini}	0.4
ρ_w	100-500 [Ωm]